

1       **Variations of Cloud Condensation Nuclei (CCN) and Aerosol**  
2       **Activity during Fog-Haze Episode: a Case Study from Shanghai**

3  
4       Chunpeng Leng <sup>a</sup>, Deqin Zhang <sup>a</sup>, Qun Zhang <sup>a</sup>, Chen Xu <sup>a</sup>, Tiantao  
5       Cheng <sup>a,b</sup>, Renjian Zhang <sup>c</sup>, Jun Tao <sup>d</sup>, Jianmin Chen <sup>a,b</sup>, Shuping Zha <sup>a</sup>,  
6       Yunwei Zhang <sup>a</sup>, Xiang Li <sup>a</sup>, Lingdong Kong <sup>a</sup>, Wei Gao <sup>e</sup>

7  
8       a. Shanghai Key Laboratory of Atmospheric Particle Pollution and  
9       Prevention (LAP<sup>3</sup>), Department of environmental science and  
10       engineering, Fudan University, Shanghai 200433, China;

11       b. Fudan-Tyndall Centre, Fudan University, Shanghai 200433, China;

12       c. Key Laboratory of Region Climate-Environment Research for  
13       Temperate East Asia, Institute of Atmospheric Physics, Chinese  
14       Academy of Sciences, Beijing 100029, China;

15       d. South China Institute of Environmental Sciences, Ministry of  
16       Environmental Protection, Guangzhou 510655, China;

17       e. Shanghai Meteorological Bureau, Shanghai 200030, China;

18  
19  
20       \* Corresponding authors: Tiantao Cheng, Jianmin Chen;

21       Tel: (86) 21-65643230; fax: (86) 21-65642080;

22       Email: [ttcheng@fudan.edu.cn](mailto:ttcheng@fudan.edu.cn), [jmchen@fudan.edu.cn](mailto:jmchen@fudan.edu.cn)

23 **Abstract**

24 Measurements of Cloud condensation nuclei (CCN), condensation nuclei  
25 (CN) and aerosol chemical composition were performed simultaneously  
26 at an urban site of Shanghai from 6 to 9 November 2010. The variations  
27 of CCN number concentration ( $N_{CCN}$ ) and aerosol activity (activated  
28 aerosol fraction,  $N_{CCN}/N_{CN}$ ) were examined during a fog-haze  
29 co-occurring event. Anthropogenic pollutants emitted from vehicles and  
30 unfavorable meteorological conditions such as low planetary boundary  
31 layer (PBL) height exerted a great influence on  $PM_{2.5}$  and black carbon  
32 (BC) loadings.  $N_{CCN}$  at 0.2% supersaturation (SS) mostly fell in the range  
33 of 994 to 6268  $cm^{-3}$ , and the corresponding  $N_{CCN}/N_{CN}$  varied between  
34 0.09 and 0.57.  $N_{CCN}$  and  $N_{CCN}/N_{CN}$  usually were higher in hazy case due  
35 to increased aerosol concentration in the accumulation mode (100-500  
36 nm), and lower in foggy-hazy and clear cases. BC mass concentration  
37 posed a strong positive effect on  $N_{CCN}$  in foggy-hazy and hazy cases,  
38 whereas it poorly correlated with  $N_{CCN}$  in clear case.  $N_{CCN}/N_{CN}$  was  
39 weakly related with BC both in foggy-hazy/hazy and clear cases. By  
40 using a simplified particle hygroscopicity ( $\kappa$ ), the calculated critical dry  
41 size (CDS) of activated aerosol did not exceed 130 nm at 0.2% SS in  
42 spite of diverse aerosol chemical compositions. The predicted  $N_{CCN}$  at  
43 0.2% SS was very successful compared with the observed  $N_{CCN}$  in clear  
44 case ( $R^2=0.96$ ) and foggy-hazy/hazy cases ( $R^2=0.91$ ). In addition, their

45 corresponding ratios of predicted to observed  $N_{CCN}$  were on average 0.95  
46 and 0.92, respectively. More organic matter is possibly responsible for  
47 this closure difference between foggy-hazy/hazy and clear cases. These  
48 results reveal that the particulate pollutant burden exerts a significant  
49 impact on  $N_{CCN}$ , especially  $N_{CCN}/N_{CN}$  promotes effectively during the  
50 polluted periods.

51 **Key words:** cloud condensation nuclei, fog, haze, aerosol, urban

52

## 53 **1. Introduction**

54 Cloud condensation nuclei (CCN), which constitutes an important  
55 fraction of atmospheric aerosol, can influence the microphysical and  
56 radiative properties and lifetime of cloud indirectly and consequently  
57 impact the hydrological cycle (IPCC, 2007). The elevated CCN loadings  
58 ( $N_{CCN}$ ) tend to reduce cloud droplet size and then suppress precipitation  
59 in shallow and short-lived clouds (Lohmann and Feichter, 2005). But it  
60 can promote great convective overturning and enhance precipitation in  
61 deep convective clouds (Rosenfeld et al., 2008). Numerous aerosol  
62 properties, including particle size distribution, chemical composition  
63 and mixing state, are closely linked with the ability of particles to take  
64 up water vapor, i.e. the ability to act as CCN (Baumgardner et al., 2003;  
65 Kuwata and Kondo, 2008; Cubison et al., 2008). To date, the current  
66 assessment of aerosol indirect effects induced by increasing

67 anthropogenic aerosols remains poorly understood, and this brings a big  
68 uncertainty in fully picturing climate change (Andreae et al., 2005;  
69 IPCC, 2007).

70 Owing to advanced instrument development, the aerosol-cloud  
71 interaction and its impact on climate have attracted increasing attention in  
72 the last decades. Many ground-based measurements on CCN have been  
73 performed in diverse environments, describing a global map of CCN  
74 distribution in the surface atmosphere (Baumgardner et al., 2003; Yum et  
75 al., 2004, 2005; Reade et al., 2006; Juranyi et al., 2010; Leng et al., 2013).  
76 In urban environments, the new particle formation and growth, and haze  
77 pollution were observed recently as having a significant impact on  $N_{CCN}$   
78 (Ritesh et al., 2007; Kuang et al., 2009). In recent years, CCN studies  
79 have raised the relative importance of several influence factors  
80 controlling aerosol CCN activity, of which size has been announced as  
81 the major factor in determining the CCN activation of aerosol particles  
82 (Dusek et al., 2006; Anttila and Kerminen, 2007; Hudson, 2007; Quinn et  
83 al., 2008; Jimenez et al., 2009; Leng et al., 2013). However, how  
84 chemical composition especially organic compounds to link with aerosol  
85 activity and then CCN has not been fully understood. In fact, up to 90%  
86 of the aerosol population has been formed by carbonaceous substances,  
87 and among them 10-70% is water-soluble (Moffet et al., 2008; Stone et  
88 al., 2008). Particularly, various externally or internally-mixed particulate

89 components comprised in urban air mass can significantly affect the  
90 CCN-sized spectra of atmospheric particles (Svenningsson et al., 2006;  
91 Reade et al., 2006; Kuwata et al., 2007). This has posed a major challenge  
92 to study aerosol composition and predict CCN activity (Hagler et al.,  
93 2007; Hings et al., 2008; Henning et al., 2010).

94 Due to rapid industrialization in Asia for decades, anthropogenic  
95 particles and relevant precursor emissions have increased significantly,  
96 and numerous studies have indicated that the increasing anthropogenic  
97 aerosol loading has significantly changed cloud microphysical and  
98 radiative properties (Streets et al., 2000, 2008; Shao et al., 2006; Wang et  
99 al., 2006; Qian et al., 2006; Rosenfeld et al., 2007; Matsui et al., 2010;  
100 Zhang et al., 2013). In China, studies on CCN have been done widely  
101 such as at polluted sites located in Yufa (Wiedensohler et al., 2009),  
102 Beijing (Yue et al., 2011), Shouxian (Liu et al., 2011) and Shanghai (Leng  
103 et al., 2013), and suburban sites in Guangzhou (Rose et al., 2010, 2011)  
104 and Wuqing (Deng et al., 2011). To our knowledge, little attention has  
105 been paid on the impacts of fog or haze on CCN and activated aerosol  
106 particles. The increases of haze occurrences are evident in the eastern and  
107 southwestern cities in China (Che et al., 2009). Shanghai is a huge  
108 metropolis in China, and the occurrence intensity of foggy and hazy days  
109 on annual time scale has been increasing gradually especially in winter  
110 (Tie and Cao, 2009), which is deeply affected by fine particle pollution

111 enhancement and possibly linked with particle hygroscopicity (Ye et al.,  
112 2011).

113 This study presents continuous measurements of CCN and aerosol  
114 during a fog-haze episode from 6 to 9 November 2010 in Shanghai. The  
115 aim is to provide insights on CCN and aerosol activity variations under  
116 fog-haze co-occurring conditions. The instrumentation and data used in  
117 the study are described in section 2. The aerosol physical and chemical  
118 properties are introduced in section 3. Section 4 presents the evolution of  
119 CCN and aerosol activity. The relationship between aerosol and CCN is  
120 discussed in section 5. Conclusions from the study are given in section 6.

## 121 **2. Methods**

### 122 **2.1 Observational Site**

123 The instruments for CCN and aerosol measurements have been  
124 mounted roughly 20 m above ground on the roof of a building in the  
125 campus of Fudan University in Shanghai (31°18'N, 121°29'E) since  
126 October 2010. The site is surrounded by populated residential and  
127 commercial areas, as well as urban streets. The East China Sea is roughly  
128 40 km east of the site, and the prevailing wind directions are  
129 southeasterly in summer and northeasterly in winter. Local time (LT)  
130 hereafter employed in this study is 8h ahead of UTC.

### 131 **2.2 Measurements and Methodology**

132  $N_{\text{CCN}}$  was measured using a continuous flow and single column CCN

133 counter (model CCN-100, Droplet Measurement Technologies, USA), in  
134 which an optical particle counter (OPC, 0.75-10 $\mu$ m) is employed to  
135 detect activated cloud droplets (Roberts and Nenes, 2005; Lance et al.,  
136 2006). The instrument was housed in an air-conditioned weather-proof  
137 container with temperature maintaining at 20°C. The ambient aerosol  
138 airflow passed through a dryer (active carbon) to lower relative humidity  
139 below 30% before entering the instrument (Leng et al., 2013). The CCN  
140 counter was calibrated using ammonium sulfate before the study, as did  
141 calibrations for temperature gradient, flow, pressure and OPC to maintain  
142 stable SS according to the DMT operation manual. In order to ensure  
143 accurately counting, zero checks were performed before and after the  
144 campaign and regularly every two months. The effective water vapor  
145 supersaturation (SS) changed alternately at 0.2% interval within 0.2-1.0%.  
146 In real atmosphere, SS varies from slightly less than 0.1% in polluted  
147 conditions to over 1.0% in clean-air stratus cloud (Hudson and Noble,  
148 2014). The selection of SS 0.2% in the present study would benefit to the  
149 measurements in the urban environment for further analysis. Although the  
150 CCN counter can operate well under conditions of particles only in a few  
151 thousand number per cubic centimeter and corrections must need for  
152 larger concentrations ( $>5000\text{cm}^{-3}$ ) (Latham and Nenes., 2011), we still  
153 used the measured  $N_{\text{CCN}}$  directly at 0.2% SS in this study since it seldom  
154 reached the upper limit.

155 A high-resolution wide-range particle spectrometer (WPS-1000 XP,  
156 MSP) was employed to observe particle size distributions in the size  
157 range of 10 nm-10  $\mu\text{m}$ . The principles of the instrument, which have been  
158 introduced in detail by Gao et al (2009), combine the Laser Light  
159 Scattering (LPS), Condensation Particle Counting (CPC) and Differential  
160 Mobility Analysis (DMA). The DMA and CPC can effectively measure  
161 aerosol particles distributed in the size range of 10-500 nm in up to 96  
162 channels. The LPS scan the size range of 350-10,000 nm in 24 additional  
163 channels. In the present study 60 channels in DMA and 24 channels in  
164 LPS for the sample mode were chosen and 3 minutes were needed to scan  
165 the entire size range completely, as it took 2 seconds for scanning each  
166 channel. DMA was calibrated with NIST SRM 1691 and SRM 1963 PSL  
167 spheres (mean diameter of 0.269 and 0.1007  $\mu\text{m}$ , respectively) to  
168 maintain DMA transfer function properly and accurate particle sizing  
169 traceable to NIST. Four NIST traceable sizes of PSL (i.e. 0.701, 1.36, 1.6  
170 and 4.0  $\mu\text{m}$ ) were used to calculate LPS. The calibration and operating  
171 methodology of WPS has been described elsewhere (Zhang et al., 2010).  
172 In addition, we have compared the aerosol size spectra measured by WPS  
173 with those measured in parallel by a calibrated scanning mobility particle  
174 sizer (SMPS, TSI 3080) with higher accuracy in the size range of 20-800  
175 nm, including size-resolved particle concentrations and peak sizes, and a  
176 strong correlation between them was derived with correlation coefficient



177  $R^2 > 0.95$  (Leng et al., 2013). The result confirms the reliability of WPS  
178 measurements for successfully characterizing the number concentration  
179 and size distribution of condensation nuclei (CN).

180 Planetary boundary layer (PBL) height and aerosol vertical  
181 extinction profile were measured using a set of micro pulse lidar (MPL)  
182 system (MPL-4B-532) with pulse energy 6-10  $\mu\text{J}$  and pulse repetition  
183 frequency 2500 Hz. The MPL is an eye safe, compact and autonomous  
184 instrument, and an effective tool used widely in the world to provide  
185 available high spatial (30 m) and temporal resolution (30 s) information  
186 of aerosol vertical distributions (Menuet et al. 1999; Cohn and Angevine,  
187 2000; Brooks, 2003). The range of lidar is roughly 30 km at night and 10  
188 km during the daytime. The description of the retrieval of aerosol  
189 parameters by the MPL will be only briefly summarized here as it has  
190 been given by He et al (2006). The vertical profile of the aerosol  
191 extinction coefficient is determined by a near end approach in solving the  
192 lidar equation (Fernald, 1984). The PBL height is determined by the MPL  
193 lidar at the altitude where a sudden decrease of scattering coefficient  
194 occurs (Boers and Eloranta, 1986). The overlap problem must be solved  
195 because it can lead to an underestimation of aerosol backscatter and  
196 extinction coefficients in the lowest altitudes having the majority of  
197 aerosols (He et al., 2006a). Outlined by Campbell et al (2002), overlap is  
198 typically solved experimentally. The system is set to point horizontally to

199 an averaged data sample with no obscuration, such as the late afternoon,  
200 when the atmosphere is well mixed and the aerosol loading is low. The  
201 backscattering over the target layer is roughly assumed constant. The  
202 similar calibration has been performed before this study.

203 An online Aethalometer (AE-31, Magee Scientific Co., Berkeley,  
204 California, USA) was employed to measure black carbon (BC) at a 5-min  
205 time resolution. The instrument was operated at an airflow rate of 5 l/min.  
206 Based on the strong absorptivity of BC to light at near infrared  
207 wavelengths (Hansen et al., 1984; Weingartner et al., 2003), BC  
208 concentration is determined using the measured light attenuation at 880  
209 nm and the appropriate value of specific attenuation cross section  
210 proportional to BC mass (Petzold et al., 1997). The attenuation can be  
211 obtained by calculating the difference between light transmission through  
212 the particle-laden sample spot and the particle-free reference spot in the  
213 filter (Cheng et al., 2006; Dumka et al., 2010). The operation, calibration  
214 and maintenance of AE-31 have been described in detail by Cheng et al.  
215 (2010).

216 An online analyzer for Monitoring Aerosols and Gases (MARGA,  
217 ADI 2080, Netherlands) was employed to measure the concentration of  
218 major inorganic water-soluble ions (e.g. Na<sup>+</sup>, K<sup>+</sup>, Mg<sup>+</sup>, Ca<sup>+</sup>, SO<sub>4</sub><sup>2-</sup>, Cl<sup>-</sup>,  
219 NO<sub>3</sub><sup>-</sup> and NH<sub>4</sub><sup>+</sup>) in ambient aerosol particles at 1-hour time resolution. An  
220 air pump controlled by a Mass Flow Controller (MFC) draws ambient air

221 with airflow of 1 m<sup>3</sup>/hour into the Sample Box. An internal calibration  
222 method by using bromide for the anion chromatograph and lithium for the  
223 cation chromatograph was operated over the entire measurement period  
224 to ensure this instrument to identify and measure ion species successfully.  
225 Instructions for the methods of sampling, operation and internal  
226 calibration have been described in detail elsewhere (Du et al., 2011).  
227 Moreover, the mass concentrations of particulate matter (PM) with  
228 aerodynamic diameter less than 2.5 μm (PM<sub>2.5</sub>), meteorological factors  
229 and atmospheric visibility were measured by a continuous PM ambient  
230 monitor (FH62C14, Thermo), an automatic weather monitoring system  
231 (HydroMet<sup>TM</sup>, Vaisala) and a automatic visibility monitor at 5-min time  
232 resolution, respectively.

### 233 **2.3 Air Mass Backward Trajectory**

234 The HYSPLIT-4 model developed by the Air Resources Laboratory  
235 (ARL) of the National Oceanic and Atmospheric Administration (NOAA),  
236 USA (Draxler et al., 2003), was employed to compute 24h air mass  
237 backward trajectories ending at 500m height (AGL) and starting at 0:00  
238 LT and 12:00 LT for each day. By doing so, we can identify aerosols from  
239 different source regions and analyze their effects on aerosol activity to  
240 compile a full view of the relation between fog-haze event and N<sub>CCN</sub>.  
241 According to these calculated trajectories plotted in Figure 1, aerosol was  
242 classified into two categories: (1) maritime aerosol transported by air

243 masses from marine areas on 6 Nov. 2010 carrying dominant oceanic  
244 particles, (2) continental aerosol in air mass traveling a long distance over  
245 inland areas on 7, 8 and 9 Nov. 2010 and carrying more anthropogenic  
246 particles (e.g. BC). Exactly, the maritime air mass originated from the  
247 China Eastern Sea, traveled northwesterly slow-moving across the  
248 Hangzhou Bay and finally arrived in Shanghai on 6 November. Then the  
249 air mass changed its pathway to southeasterly at around 12:00 am on 7  
250 November, and originated from northern inland areas and traveled across  
251 the North China Plain (NCP) and the eastern region of China. The  
252 continental sources contained increasing industrial and agricultural  
253 emissions (e.g. biomass burning) due to long-term rapid economy growth  
254 and large population in the last few decades. We hope to better  
255 understand the impact of aerosols with or without anthropogenic  
256 particulate pollutants on CCN in this study by comparing these two  
257 categories.

## 258 **3. Results**

### 259 **3.1 Overview of the Fog-haze Event**

260 Haze is traditionally defined as an atmospheric phenomenon that the  
261 sky clarity is obscured by dust, smoke and other dry particles, and  
262 atmospheric visibility and relative humidity (RH) are usually less than 10  
263 km and 80% over one haze episode (Fu et al., 2008). The high frequency  
264 of haze or hazy days is observed in winter, especially in the urban

265 environments of northern China (Sun et al., 2006). During the haze event,  
266 the enhancement of particulate pollutants may greatly affect aerosol  
267 activity and  $N_{CCN}$ . The study performed in the Indo-Gangetic plain shows  
268 that winter haze exerts a significant impact on the fog and low-cloud  
269 formation (Gautam et al., 2007). Fog can be viewed as a  
270 lower-atmospheric near-surface cloud, and plays an important role in  
271 processing aerosol particles and trace gases (Gultepe et al., 2007; Biswas  
272 et al., 2008). On one hand, physically similar to cloud droplet, fog droplet  
273 also forms by water vapor condensing on dry aerosol particle under  
274 supersaturated conditions. On the other hand, generally formed in the  
275 shallow boundary layer containing local emissions, urban fog traps more  
276 pollutants than cloud at high altitudes (Fisak et al., 2002; Herckes et al.,  
277 2007). The fog or foggy case is defined as a weather with patterns of low  
278 visibility (<10 km) and higher RH (>90%). When  $80\% < RH < 90\%$ , the  
279 weather was referred as a complex of haze and fog co-occurring (e.g.  
280 foggy-hazy) in the present study. Figure 2 and 3 show a 4-day time series  
281 of pressure, atmospheric visibility, RH, temperature, wind speed and  
282 direction, and PBL height from 6 to 9 November 2010. In fact, since RH  
283 seldom reached up to 90%, thus the period focused in the present study  
284 were characterized as hazy and foggy-hazy cases. The haze pollution  
285 lasting at least 4 hours has been identified as one haze event by an earlier  
286 study in Shanghai, where authors paid attention to the formation of haze

287 pollution (Du et al., 2011).

288 As shown in Figure 2-8, the 4-day period was classified into three parts:  
289 a hazy episode (marked in black open boxes) from 22:00 to 23:00 LT on 6  
290 Nov. and 10:00 LT on 7 Nov. to 13:00 LT on 8 Nov., a foggy-hazy  
291 episode (marked in red open boxes) from 23:00 LT on 6 Nov. to 10:00 LT  
292 on 7 Nov., and the rest for clear episode. Statistics for meteorological  
293 conditions is listed in Table 1. During the hazy and foggy-hazy case, the  
294 average atmospheric visibility was about 4.44 km and 2.33 km,  
295 respectively, much lower than 15.4 km in the clear case. The winds from  
296 the east and the south brought clean maritime aerosol during the clear  
297 case, however, the winds from the north and the west brought polluted  
298 anthropogenic aerosol during the hazy and foggy-hazy cases. The  
299 particulate and gaseous matters, including pollutants (e.g. BC) emitted  
300 from agricultural biomass burning were transported along the air mass  
301 pathways (Figure 1), led to a significant enhancement of aerosol  
302 extinction coefficient (Figure 3). In addition, the PBL height downed to  
303 below 500 m and further suppressed the dilution of pollutants.

### 304 **3.2 Physical and Chemical Properties of Aerosol**

305 In order to visually identify aerosol evolution, particles in the size  
306 range of 10 nm to 10  $\mu\text{m}$  were categorized into 7 sub-size bins: 10-20 nm  
307 (nucleation mode), 20-50nm and 50-100nm (Aitken mode), 100-200nm,  
308 200-500nm and 0.5-1  $\mu\text{m}$  (accumulation mode), and 1-10  $\mu\text{m}$  (coarse

309 mode) (Figure 4). The similar classification has been done in the  
310 measurements at the same site by Zhang et al (2010). In this study, the  
311 integrated particle size-resolved number concentrations ( $N_{CN}$ ) exhibited a  
312 regular diurnal cycle, with two peaks (9,000-16,000  $cm^{-3}$ ) almost within  
313 the traffic rush hours. The mean  $N_{CN}$  exhibited no obvious difference  
314 between the foggy-hazy (8,367  $cm^{-3}$ ) and clear (8,956  $cm^{-3}$ ) cases, but it  
315 showed a higher value (10,500  $cm^{-3}$ ) in the hazy cases, revealing a larger  
316 loading of particulate pollutants.

317 In general, the 20-100 nm (Aitken mode) particles are mostly  
318 dominant in all size particles probably due to local traffic emissions and  
319 meteorological conditions (Ferin e al., 1990). The temporal variation  
320 trend of Aitken mode was similar to  $N_{CN}$ . It was interesting that the  
321 particles of 100-500 nm (accumulation mode) dominated in  $N_{CN}$  in the  
322 hazy case with peak concentrations higher than 7,500  $cm^{-3}$ , almost twice  
323 as much as the clear case (4,000  $cm^{-3}$ ). However, the foggy-hazy case is  
324 comparable to the clear case, showing a mostly unchanged evolution of  
325 the fractions of individual size bin to total particles and  $N_{CN}$ . In addition,  
326 Figure 5 shows the average size distributions for all the three cases. It is  
327 very visible that it contains relatively more large-sized (e.g. 100 nm)  
328 aerosol particles in the aerosol population during the hazy case than that  
329 during the clear and foggy-hazy cases. Especially aerosol particles larger  
330 than 200 nm (a typical CCN size at SS 0.2%) were significantly

331 enhanced.

332 Figure 6 shows the temporal variations of eight major inorganic water  
333 soluble ions in aerosol particles and four gaseous pollutants sampled  
334 during this study period. Measurements for  $\text{SO}_4^{2-}$ ,  $\text{Cl}^-$  and  $\text{NO}_3^-$  were  
335 unavailable from 10:00 LT on 7 Nov. to 8:00 LT on 8 Nov. Substantially,  
336 the average concentration of aerosol total water soluble ions (TWSI) in  
337 the hazy case ( $54.52 \mu\text{g m}^{-3}$ ) was comparable to the foggy-hazy case  
338 ( $50.37 \mu\text{g m}^{-3}$ ), and roughly 2 times that of the clear case ( $26.22 \mu\text{g m}^{-3}$ ).  
339 For the percentage of individual ions in TWSI,  $\text{NH}_4^+$  and  $\text{K}^+$  were  
340 relatively higher by a factor of 1.8 in the hazy and foggy-hazy cases than  
341 in the clear case. Despite the lack of  $\text{SO}_4^{2-}$  and  $\text{NO}_3^-$  partly during the  
342 hazy case, we can still conjecture their promotion on the basis of their  
343 gaseous precursor evolution of  $\text{SO}_2$  and  $\text{NO}_2$ .

344 Gaseous pollutants are released into the atmosphere from natural and  
345 anthropogenic emissions. Among them,  $\text{SO}_2$  is known as one of the most  
346 important gaseous pollutants and a precursor responsible for acid rain.  
347 Also, it can participate in the formation of new particles through  
348 converting into gaseous  $\text{H}_2\text{SO}_4$ , which is the most common nucleation  
349 species due to its low vapor pressure at typical atmospheric temperature  
350 (Zhang et al., 2006b; Urone et al., 1968). Secondary aerosols produced  
351 from the formation of new particles contribute more to the global aerosol  
352 burden than primary aerosols and are important sources of CCN



353 (Merikanto et al., 2009; Yu et al., 2008). Recent studies have shown the  
354 enhanced solubility of SO<sub>2</sub> due to its reaction in fog droplets during a  
355 severe fog measured in the North China Plain, and this finding has  
356 provided important support for better understanding of the acidity in  
357 clouds (Zhang et al., 2013). NO<sub>2</sub> mainly comes from vehicle traffic  
358 emissions in urban areas (Wang et al., 2006). Nitrogen oxides (NO, NO<sub>2</sub>,  
359 N<sub>2</sub>O<sub>5</sub>) undergo heterogeneous reactions with aerosol particles (e.g. sea  
360 salt or dust) during they are transported in the atmosphere (Elizabeth et  
361 al., 2006). Thus, high gaseous pollutant content can result in larger CN  
362 loadings and subsequently more CCN particles in the atmosphere. On the  
363 whole, the loading of these precursor gases in the foggy-hazy and hazy  
364 cases exceeded that in the clear case, specifically NO<sub>2</sub> by a factor of 2 and  
365 SO<sub>2</sub> by a factor of 1.5. Moreover, SO<sub>2</sub> and NO<sub>2</sub> concentrations reached  
366 their peaks around 0:00 LT on 8 November corresponding to the highest  
367 levels of CCN and aerosol activity, implying their potential effects on  
368 CCN production, which will be discussed in the next section.

### 369 **3.3. CCN Concentration and Aerosol Activity**

#### 370 **3.3.1 CCN and Aerosol Activity**

371 Figure 7 presents the temporal variations of N<sub>CCN</sub> and activated  
372 aerosol fraction (N<sub>CCN</sub>/N<sub>CN</sub>) at SS 0.2%, N<sub>CN</sub>, and BC during the  
373 campaign. Totally, N<sub>CN</sub> fell in the range of 4,270-15,771 cm<sup>-3</sup> and  
374 averaged at 9,344 cm<sup>-3</sup>, and N<sub>CCN</sub> varied between 994 cm<sup>-3</sup> and 6,268 cm<sup>-3</sup>

375 and averaged at  $2,929 \text{ cm}^{-3}$ . High  $N_{\text{CCN}}/N_{\text{CN}}$  (0.41) and  $N_{\text{CCN}}$  ( $4,362 \text{ cm}^{-3}$ )  
376 were observed during the hazy case, followed by the foggy-hazy (0.29,  
377  $2,377 \text{ cm}^{-3}$ ) and clear (0.28,  $2,432 \text{ cm}^{-3}$ ) cases (Table 2). The temporal  
378 variation of  $N_{\text{CCN}}/N_{\text{CN}}$  and  $N_{\text{CCN}}$  was closely related with aerosol  
379 particle size spectra and chemical composition such as accumulation  
380 mode (100-500 nm) and water soluble ion content (Figure 4 and 6).  
381 Figure 8 gives the temporal variations of number concentrations of larger  
382 aerosol particles (e.g. particles larger than 80 nm and 100 nm) and their  
383 corresponding ratios with  $N_{\text{CCN}}$  at SS 0.2%. The larger aerosol particles  
384 showed significant increase during the hazy case and varied strongly  
385 correlated with  $N_{\text{CCN}}$ . More fractions of particles larger than 80 nm were  
386 activated into CCN during the hazy case (86%) and foggy-hazy case  
387 (84%) than that during the clear case (76%).

388 Although in different SS conditions,  $N_{\text{CCN}}$  was measured at other urban  
389 or urban-like environments such as the west coast of Tasmania ( $32 \text{ cm}^{-3}$ )  
390 and the west coast of Korea ( $5,292 \text{ cm}^{-3}$ ) at SS 1.0% (Yum et al., 2004,  
391 2005), and Mexico city ( $3,000 \text{ cm}^{-3}$ ), Ireland (208-346  $\text{cm}^{-3}$ ) and Vienna  
392 ( $820 \text{ cm}^{-3}$ ) at SS 0.5% (Baumgardner et al., 2003; Reade et al., 2006;  
393 Burkart et al., 2011). An even larger  $N_{\text{CCN}}$  ( $6,000 \text{ cm}^{-3}$ ) was measured at  
394 SS 0.17% in Beijing (Deng et al., 2011). The average  $N_{\text{CCN}}/N_{\text{CN}}$  of this  
395 study (0.32) was higher than that measured in Vienna (0.13 at SS 0.5%,  
396 CN 13-929 nm) and Finland (0.1-0.3 at SS 0.2%, CN 3-1000 nm). The

397 increased  $N_{CCN}/N_{CN}$  was derived at larger SS in urban environments such  
398 as Shanghai (0.47 at SS 0.8%, CN 10-10,000 nm) and Korea (0.64 at SS  
399 1.0%, CN 10-500 nm) (Yum et al., 2005; Burkart et al., 2011; Sihto et al.,  
400 2011; Leng et al., 2013).

401 As expected,  $N_{CN}$  behaved in diurnal cycle with an apparent pattern of  
402 bi-modal distribution, and  $N_{CCN}$  showed a similar temporal variation  
403 (Figure 7).  $N_{CN}$  and BC usually peaked, and reached their highest values  
404 of  $15,000 \text{ cm}^{-3}$  and  $35 \mu\text{g m}^{-3}$  during the rush hours (i.e. 7:00-9:00 and  
405 16:00-19:00 LT), indicating that the anthropogenic pollutants emitted  
406 from vehicles contributes to a large part of CN and BC loadings. In  
407 addition, the favorable meteorological conditions such as low wind speed,  
408 temperature and planetary boundary layer (PBL) height also posed a great  
409 influence on  $\text{PM}_{2.5}$  and BC loadings (Figure 3). For example,  $\text{PM}_{2.5}$  and  
410 BC accumulated in mass concentration and reached their maximums  
411 when these meteorological parameters remained at low level (e.g. wind  
412 speed at  $2 \text{ m s}^{-1}$ , PBL height around 0.5 km. The later disappearance of  
413 the pollutants at the end of the hazy case was mostly attributed to the  
414 wind speed increasing from 2 to  $6 \text{ m s}^{-1}$ , and the PBL height rising from  
415 0.4 to 1.4 km (Figure 2).

416 In a broad view,  $N_{CCN}$  showed a sharp increase starting at 0:00 LT on 8  
417 Nov., and rose from  $994 \text{ cm}^{-3}$  to  $6268 \text{ cm}^{-3}$  within less than 10 hours.  
418 Similar to  $N_{CCN}$ , BC also rose from  $10 \mu\text{g m}^{-3}$  to  $35 \mu\text{g m}^{-3}$  during the

419 same period.  $N_{\text{CN}}$  was consistent with  $N_{\text{CCN}}$ , and they varied almost  
420 synchronously. However,  $N_{\text{CCN}}/N_{\text{CN}}$  changed in one step mostly opposite  
421 to  $N_{\text{CCN}}$  and  $N_{\text{CN}}$  (Figure 7). The possible reason for this contradictory  
422 tendency of  $N_{\text{CN}}$  enhancement vs.  $N_{\text{CCN}}/N_{\text{CN}}$  reduction is that the  
423 unactivated nanoparticles, which burst partly from primary emissions of  
424 vehicles and/or partly from secondary particles due to the chemical  
425 reactions of atmospheric gaseous precursors (Figure 5) (Du et al., 2011),  
426 contributes relatively larger to  $N_{\text{CN}}$  other than  $N_{\text{CCN}}$ .

### 427 **3.3.2 Black Carbon and CCN**

428 As a part of hydrophobic aerosols, pure BC particles acquire  
429 hydrophilic coatings as they age in the atmosphere, and then the aged BC  
430 becomes sufficiently hydrophilic and serves as CCN for cloud  
431 condensation formation (Ritesh et al., 2007). On the other hand, BC  
432 particles can release sensible heat by effectively absorbing solar radiation,  
433 thereby increasing the critical supersaturation of CCN and preventing  
434 aerosol to act as CCN (Conant et al., 2002). Biomass burning emits a  
435 large amount of trace gases and carboneous particles into the atmosphere,  
436 and leads to changes in climate and precipitation, as well as aquatic and  
437 terrestrial ecosystem (Andreae et al., 2004). The wild fires contribute a  
438 significant fraction of global CCN burden (Pierce et al., 2007; Andreae et  
439 al., 2009). Large quantities of active agricultural fire sites were detected  
440 from satellites over China on 7 November 2010 (Figure 1), whereas no

441 obvious wild biomass burning activities were observed during the rest  
442 days. Based on the calculated 24-h air mass backward trajectories, the air  
443 mass that passed right through the agricultural fire regions in the Jiangsu  
444 and Anhui provinces on 7 November reached the sampling site in the next  
445 day, bringing large quantities of aged BC particles after a long range  
446 transport. This resulted in a severe increase of particle mass concentration  
447 and a significant enhancement of aerosol extinction coefficient on 7 and 8  
448 November (Figure 3). As discussed in section 3.2,  $\text{NO}_2$  and  $\text{SO}_2$   
449 concentrations increased synchronously during the whole period (Figure  
450 6), and they would undergo heterogeneous reactions on the surface of BC  
451 particles to change particle microphysical and chemical properties,  
452 making BC particles sufficiently hydrophilic to act as CCN (Ritesh et al.,  
453 2007).

454 Relationship analyses between  $N_{\text{CCN}}$ ,  $N_{\text{CCN}}/N_{\text{CN}}$  and BC were  
455 calculated using hourly-averaged data, and the correlation coefficients ( $R^2$ )  
456 are presented in Figure 9. Surprisingly, BC strongly correlated with  $N_{\text{CCN}}$   
457 ( $R^2=0.85$ ) in the foggy-hazy and hazy cases, whereas they showed a poor  
458 linear relationship ( $R^2=0.25$ ) in the clear case. The possible reason is BC  
459 particle aging by heterogeneous reactions with gaseous pollutants (e.g.  
460  $\text{NO}_2$  and  $\text{SO}_2$ ) to be activated CCN during pollutant atmospheric transport  
461 (Ritesh et al., 2007). In addition, so many studies have proposed that the  
462 aged BC is efficient CCN (Dusek. et al., 2006; Anttila and Kerminen,

463 2007; Hudson, 2007). However,  $N_{CCN}/N_{CN}$  was poorly related with BC  
464 for both foggy-hazy/hazy and clear cases ( $R^2=0.43$  and  $0.07$ , respectively),  
465 indicating that BC maybe a relatively more important contributor to  
466 unactivated particles especially in nanoscale sizes (e.g. traffic emission)  
467 than activated CCN.

### 468 **3.4. Relationship of Aerosol and CCN**

469 Although aerosol size distributions were measured only in the size  
470 range of 10-10,000 nm, they were still used to predict  $N_{CCN}$  according to  
471 Köhler theory (Köhler et al., 1936). Toward this end, the particle  
472 hygroscopicity “kappa” ( $\kappa$ ) was used in the closure calculation. The  
473 description of the technique has been given by Petters and Kreidenweis  
474 (2007), therefore it will only be briefly summarized here. The  $\kappa$   
475 parameter for one multicomponent particle can be obtained through  
476 weighting each component  $\kappa_i$  by their volume fractions in the mixture,

$$477 \quad \kappa = \sum_i \varepsilon_i \kappa_i \quad (1)$$

478 where  $\varepsilon_i$  is the volume fraction of chemical compounds in particles,  
479 and  $\kappa_i$  is the effective  $\kappa$  of individual chemical composition.

480 Assuming aerosol particles are completely internal-mixed, a simplified  
481  $\kappa$  was calculated using water soluble inorganic ions (organic matter data  
482 is unavailable). Aerosol particle compositions were classified into three  
483 categories (Petters and Kreidenweis, 2007; Wiedensohler et al., 2009),  
484 and  $\kappa_i$  and densities for each component are shown in Table 3, in which

485 ‘others’ is defined as ‘PM<sub>2.5</sub>-BC-inorganic ions’. The critical dry size  
486 (CDS) of particle to be activated as CCN at one SS can hence be  
487 determined by the following equation:

$$488 \quad S(D) = \frac{D^3 - D_d^3}{D^3 - D_d^3(1 - \kappa)} \exp\left(\frac{4\sigma_{s/a}M_w}{RT\rho_w D}\right) \quad (2)$$

489 where  $\rho_w$  is the density of water,  $M_w$  is the molecular weight of water,  
490  $\sigma_{s/a}$  is the surface tension of the solution/air interface,  $R$  is the universal  
491 gas constant,  $\kappa$  is the hygroscopicity parameter,  $T$  is temperature,  $D_d$  is the  
492 dry diameter,  $D$  is the diameter of the droplet and  $S(D)$  is the critical dry  
493 size under a given SS. Detailed information for the derivation of equation  
494 (2) can be found in Petters and Kreidenweis (2007). Equation (2) applies  
495 over the entire range of humidity and solution hygroscopicity and can be  
496 utilized to predict the conditions of cloud droplet activation. The critical  
497 SS for a selected dry size of particle is determined from the maximum of  
498 the curve for equation (2). Computed for  $\sigma_{s/a}=0.072 \text{ J m}^{-2}$  and  $T=298.15 \text{ K}$ ,  
499 the calculated CDS varied between 60 nm and 130 nm and averaged at  
500 102 nm. Particularly, the hourly-averaged CDS during the  
501 foggy-hazy/hazy cases was slightly lower (96 nm) than during the clear  
502 case (105 nm). So far, the comparable or relatively higher CDS has also  
503 been found in diverse regions and for various aerosol types, despite of  
504 different calculation models and SS. For example, the fresh aerosol  
505 particles emitted by an aircraft internal combustion engine have a CDS  
506 range of 146-301 nm at SS 0.7%, depending on varying operating

507 conditions (Hitzenberger et al., 2003). Furutani et al (2008) investigated  
508 three types of aerosol masses along the southern coast of California, and  
509 the CDS was estimated at 110 nm at SS 0.6% for fresh ship exhaust,  
510 70-110 nm for fresh anthropogenic aerosols and roughly 50 nm for aged  
511 anthropogenic and clean maritime aerosols. In Vienna, the CDS has a  
512 wide gap between 69 nm and 368 nm, and averaged at 169 nm (Burkart et  
513 al., 2011). Quinn et al (2008) observed the CDS in a narrow range of 70-  
514 90 nm for maritime aerosols in the Gulf of Mexico, and a moderate range  
515 of 90-170 nm in the ship channels of Houston with high marine traffic  
516 densities close to industrial and anthropogenic sources.

517 The CCN population can be effectively viewed as a subset of measured  
518 aerosol size distributions since the operating range (10-10,000 nm)  
519 includes the majority of atmospheric particles. Therefore, the predicted  
520  $N_{CCN}$  can be calculated through integrating particles upward in size from  
521 the bottom CDS to the upper boundary. In this calculation, the predicted  
522  $N_{CCN}$  of hourly-averaged were compared with the measured ones  
523 correspondingly.

524 The results of this closure analysis are shown in scatterplot in Figure  
525 10 and 11. The prediction for CCN is generally success throughout the  
526 entire data set. The linear regression between predicted and measured  
527  $N_{CCN}$  produces a slope of 1.012 and an intercept of  $128.3 \text{ cm}^{-3}$  ( $R^2=0.95$ ),  
528 and the average ratio of predicted versus measured  $N_{CCN}$  is 0.94 (Figure



529 10). The results indicate some moderate underestimate (about 6% on  
530 average) but the agreement is still excellent. The achieved closure  
531 calculation suggested that water soluble inorganic ions played a major  
532 role in contributing the  $\kappa$  value. In fact, 83.8% of the  $\kappa$  was expressed  
533 by  $\text{SO}_4^{2-} + \text{NO}_3^- + \text{NH}_4^+$  in total (in another study by our group, not  
534 published yet), with their individual contribution to be 39.8%, 31.7%  
535 and 12.3%, respectively. In addition, it is worth note that the predicted  
536  $N_{\text{CCN}}$  at SS 0.2% was more correlated with the observed  $N_{\text{CCN}}$  in the clear  
537 case ( $R^2=0.96$ ) than the foggy-hazy/hazy cases ( $R^2=0.91$ ), and the  
538 corresponding ratios of predicted to observed  $N_{\text{CCN}}$  were 0.95 and 0.92,  
539 respectively (Figure 11). In all cases, the mean ratio of predicted to  
540 observed  $N_{\text{CCN}}$  never reached up to 1, suggesting that organic matter  
541 would play a second role and make up the rest of  $\kappa$ .

#### 542 **4. Conclusions and discussion**

543 A continuous 4-day data obtained at an urban site of Shanghai over a  
544 fog-haze event from 6 to 9 November 2012 was analyzed for CCN and  
545 aerosol. Overall, meteorological conditions such as wind speed, wind  
546 direction and temperature exerted a great influence on  $\text{PM}_{2.5}$  and BC  
547 loadings. Human activity is an essential factor to control emissions of  
548 aerosol and CCN in urban environments.  $N_{\text{CCN}}/N_{\text{CN}}$  and  $N_{\text{CCN}}$  usually  
549 were higher in the hazy case due to increased aerosols in the  
550 accumulation mode, and lower in the foggy-hazy and clear cases. Of

551 special interest, the low  $N_{CCN}/N_{CN}$ ,  $N_{CN}$  and  $N_{CCN}$  during the foggy-hazy  
552 case can plausibly explain in three aspects: (1) the limited data input  
553 introduces some uncertainties, (2) the possible physical effects such as  
554 boundary layer evolution, transportation and atmospheric dilution (i.e. the  
555 effect of diurnal variations) are not considered, (3) the plausible  
556 emergence of fog droplets and particles leads to the reduction of aerosol  
557 number concentration.

558 BC was correlated well with  $N_{CCN}$  in the foggy-hazy and hazy cases  
559 but the clear case, as not  $N_{CCN}/N_{CN}$  did. More BC is aged during the  
560 foggy-hazy/hazy cases, hence more CCN is activated (Dusek et al., 2006;  
561 Anttila and Kerminen., 2007; Hudson., 2007). However, there exists a  
562 different perspective. For example, BC has been found to significantly  
563 suppress cloud formation in the Indo-Gangetic plain (Ritesh et al., 2007).  
564 Pure BC particles are hydrophobic and can release heat by absorbing  
565 solar radiation, hence they would increase the critical SS of aerosol to act  
566 as CCN and further suppress the tendency of CCN to become cloud  
567 droplets. However, aged BC particles are sufficiently hydrophilic by  
568 acquiring hydrophilic coatings in the atmosphere, and become CCN and  
569 favor aerosol indirect forcing (Conant et al., 2002; Ritesh et al., 2007). In  
570 this study, BC particles moved a long-distance from inland and aged  
571 during the transporting process, thereby it favors CCN formation.

572 By using a simplified  $\kappa$  parameter, the critical dry size never exceeded

573 130 nm. In spite of the absence of organic matter, the CCN closure  
574 calculation was still achieved, suggesting that aerosol major water soluble  
575 ions contribute to effective  $\kappa$ . The predicted  $N_{CCN}$  was close to the  
576 observed during the clear case than the foggy-hazy/hazy cases  
577 having more organic matter. In summary, water soluble inorganic  
578 ions constituted the majority of particle hygroscopicity ( $\kappa$ ) estimation,  
579 while organic matter made up the rest. It is noted that organic matter is  
580 essential to build the exact CCN prediction models.

581 This paper mainly explored how  $N_{CCN}$ ,  $N_{CN}$  and  $N_{CCN}/N_{CN}$  vary under a  
582 fog-haze co-occurring condition, as well as the major influential factors  
583 to these activities. The results revealed that the particulate pollutant  
584 burden exerts a significant impact on  $N_{CCN}$ , especially  $N_{CCN}/N_{CN}$  is  
585 effectively promoted during the polluted periods (e.g. haze). Importantly,  
586 the fog-haze transformation is highly complicated involving numerous  
587 changes of aerosol in physical and chemical properties, which remains  
588 poorly understood. There presents the results of only a case, so more  
589 efforts are needed for highlighting the comprehensive effects of fog and  
590 haze on CCN in urban environments.

591

## 592 **Acknowledgements**

593 This research is supported by the National Basic Research Program of  
594 China (2010CB428503), the National Natural Science Foundation of

595 China (41075096, 21190053, 21177025, 21277028, 21377029,  
596 41475109), and partly by the Research and Development Special Fund  
597 for Public Welfare Industry (Meteorology) of CMA (GYHY201006047),  
598 the Shanghai Science and Technology Commission of Shanghai  
599 Municipality (12DJ1400100, 12DZ2260200), the Jiangsu Collaborative  
600 Innovation Center for Climate Change, and Priority fields for Ph.D.  
601 Programs Foundation of Ministry of Education of China (0110071130003)  
602 and FP7 project (AMIS, PIRSES-GA-2011).

603

## 604 **Reference**

605 Andreae, M. O., et al.: Correlation between cloud condensation nuclei  
606 concentration and aerosol optical thickness in remote and polluted  
607 regions, *Atmos. Chem. Phys.*, 9, 543-556, doi: 10.5194/acp-9-543-2009,  
608 2009.

609 Andreae, M. O., et al.: Smoking rain clouds over the Amazon, *Science.*,  
610 303, 1337-1342, doi: 10.1126/science. 1092779,2004.

611 Andreae, M. O., Jones, C. D., and Cox. P. M.: Strong present-day aerosol  
612 cooling implies a hot future, *Nature.*, 435, 1187-1190, 2005.

613 Anttila, T., and Kerminen, V. M.: On the contribution of Aitken mode  
614 particles to cloud droplet populations at continental back-ground areas-a  
615 parametric sensitivity study, *Atmos. Chem. Phys.*, 7, 4625-4637, 2007.

616 Baumgardner, D., Raga, G. B., and Muhlia, A.: Evidence for the

617 formation of CCN by photochemical processes in Mexico City, Atmos.  
618 Environ., doi:10.1016, 2003.

619 Biswas, K. F., Ghauri, B. M., and Husain, L.: Gaseous and aerosol  
620 pollutants during fog and clear episodes in South Asian urban  
621 atmosphere, Atmos. Environ., 42, 7775-7785, 2008.

622 Boers, R., and Eloranta, E.W.: Lidar measurements of the atmospheric  
623 entrainment zone and the potential temperature jump across the top of  
624 the mixed layer, Boundary-Layer Meteorology, 34, 357-375, 1986.

625 Brooks, I.M.: Finding boundary layer top: application of a wavelet  
626 covariance transform to lidar backscatter profiles, Journal of  
627 Atmospheric and Oceanic Technology, 20, 1092-1105, 2003.

628 Burkar, J., Steiner, G., Reischl, G., and Hitzenberger, R.: Long-term study  
629 of cloud condensation nuclei (CCN) activation of atmospheric aerosol in  
630 Vienna, Atmos. Environ., 45, 5751-5759, 2011.

631 Campbell, J.R., Hlavka, D.L., Welton, E.J., Flynn, C.J., Turner, D.D.,  
632 Spinhirne, J.D., Scott, V.S., and Hwang, I.H.: Full-time, eye-safe cloud  
633 and aerosol lidar observation at atmospheric radiation measurement  
634 program sites: Instruments and data processing, J. Atmos. Oceanic  
635 Technol., 19, 431-442, 2002.

636 Che, H. Z., Zhang, X. Y., Li, Y., Zhou, Z. J., Qu, John. J and Hao, X. J.:  
637 Haze trends over the capital cities of 31 provinces in China, 1981-2005,  
638 Theor. Appl. Climatol., 97, 235-242, 2009.

639 Cheng, T. T., Han, Z. W., Zhang, R. J., Du, H. H., Jia, X., Wang, J. J., and  
640 Yao, J. Y.: Black carbon in a continental semi-arid area of Northeast  
641 China and its possible sources of fire emission, *J. Geophys. Res.*, 115,  
642 D23204, doi: 10.1029/2009JD013523, 2010.

643 Cheng, Y., Lee, S. C., Ho, K. F., Wang, Y. Q., Cao, J. J., Chow, J. C., and  
644 Watson, J. G.: Black carbon measurement in a coastal area of south  
645 China, *J. Geophys. Res.*, 111, D12310, doi: 10.1029/2005JD006663,  
646 2006.

647 Cohn, S.A., Angevine W.M.: Boundary layer height and entrainment zone  
648 thickness measured by lidars and wind-profiling radars. *Journal of*  
649 *Applied Meteorology*, 39, 1233-1247, 2000.

650 Conant, W. C., A. Netes, and J. H. Seinfeld.: Black carbon radiative  
651 heating effect on cloud microphysics and implications for the aerosol  
652 indirect effect: 1. Extended Köhler theory, *J. Geophys. Res.*, 107 (D21),  
653 4604, doi:10.1029/2002JD002094, 2002.

654 Cubison, M. J., Ervens, B., Feingold, G., Docherty, K. S., Ulbrich, I. M.,  
655 Shields, L., Prather, K., Hering, S. and Jimenez, J. L.: The influence of  
656 chemical composition and mixing state of Los Angeles urban aerosol on  
657 CCN number and cloud properties, *Atmos. Chem. Phys.*, 8, 5649-5667,  
658 2008.

659 Deng, Z. Z., Zhao, C. S., Ma, N.P., Liu, F., Ran, L., Xu, W. Y., Liang, Z.,  
660 Liang, S., Huang, M. Y., Ma, X.C., Zhang, Q., Quan, J. N., and Yan, P.:

661 Size- resolved and bulk activation properties of aerosols in the North  
662 China Plain, *Atmos. Chem. Phys.*, 11, 3835-3846, 2011.

663 Draxler, R. R., and Rolph, G. D.: HYSPLIT(Hybrid Single-Particle  
664 Lagrangian Integrated Trajectory) Model access via NOAA ARL  
665 READY Website (<http://www.arl.noaa.gov/ready/hysplit4.htm>), NOAA  
666 Air Resources Laboratory, Silver Spring, MD, 2003.

667 Du, H., Kong, L., Cheng, T., Chen, J., Du, J., et al.: Insights into  
668 summertime haze pollution events over Shanghai based on online  
669 water-soluble ionic composition of aerosols, *Atmos. Environ.*, 45,  
670 5131-5137, 2011.

671 Dumka, U.C., Krishna Moorthy, K., Rajesh Kumar, Hegde, P., Ram Sagar,  
672 Pant, P., et al.: Characteristics of aerosol black carbon mass  
673 concentration over a high altitude location in the Central Himalayas  
674 from multi-year measurements, *Atmos. Res.*, 96, 510-521, 2010.

675 Dusek, U., Frank, G. P., and Hildebrandt, L.: Size matters more than  
676 chemistry for cloud- nucleating ability of aerosol particles, *Science*, 312,  
677 1375-1378, 2006.

678 Elizabeth, R. G., Paula, K. H., and Vicki, H. G.: Physicochemical  
679 properties of nitrate aerosols: Implications for the atmosphere, *J. Phys.*  
680 *Chem.*, 110, 11785-11799, 2006.

681 Ferin, J., Oberdoerster, G., Penney, D. P., Soderholm, S. C., Gelein, R.,  
682 and Piper, H. C.: Increased pulmonary toxicity of ultrafine particles 1.

683 Particles clearance, translocation, morphology, *J. Aerosol Sci.*, 21 (3),  
684 381-384, 1990.

685 Fernald, F. G.: Analysis of atmospheric lidar observations: Some  
686 comments, *Appl. Opt.*, 23(5), 652-653, 1984.

687 Fisak, J., Tesar, M., Rezacova, D., Elias, V., Weignerova, V., and Fottova,  
688 D.: Pollutant concentrations in fog and low cloud water at selected sites  
689 of the Czech Republic, *Atmos. Res.*, 64, 75-87, 2002.

690 Fu, Q. Y., Zhuang, G. S., Wang, J., Xu, C., Huang, K., Li, J., Hou, B., Lu,  
691 T., and Streets, D. G.: Mechanism of formation of the heaviest  
692 pollution episode ever recorded in the Yangtze River Delta, China,  
693 *Atmos. Environ.*, 42, 2023-2036, 2008.

694 Furutani. H., Dall'Osto, M., Roberts, G. C., and Prather, K. A.:  
695 Assessment of the relative importance of atmospheric aging on CCN  
696 activity derived from field observations, *Atmos. Environ.*, 42,  
697 3130-3142, 2008.

698 Gao, J., Wang, T., Zhou, X. H., Wu, W. S., and Wang, W. X.:  
699 Measurement of aerosol number size distributions in the Yangtze River  
700 delta in China: formation and growth of particles under polluted  
701 conditions, *Atmos. Environ.*, 43 (4), 829-836, 2009.

702 Gautam, R., Hsu, N. C., Kafatos, M. and Tsay, S. C.: Influences of winter  
703 haze on fog/low cloud over the Indo-Gangetic plains, *J. Geophys. Res.*,  
704 112, D05207, doi: 10.1029/2005JD007036, 2007.



705 Gulpete, I., Tardif, R., Michaelides, S. C., Cermak, J., Bott, A., Bendix, J.,  
706 Müller, M. D., Pagowski, M., Hansen, B., Ellrod, G., Jacobs, W., Toth,  
707 G., and Cober, S. G.: Fog research: a review of past achievements and  
708 future perspectives, *Pure and Applied Geophys.*, 164, 1121-1159, 2007.

709 Hagler, G. S. W., Bergin, M. H., Smith, E. A. and Dibb, J. E.: A summer  
710 time series of particulate carbon in the air and snow at Summit,  
711 Greenland, *J. Geophys. Res.*, 112, D21309, doi: 10.1029/2007JD008993,  
712 2007.

713 Hansen, A. D. A., Rosen, H., and Novakov T.: The aethalometer-an  
714 instrument for the real-time measurement of optical absorption by  
715 aerosol particles, *Sci. Total Environ.*, 36, 191-196, 1984.

716 He, Q. S., Li, C. C., Mao, J. T., Lau, A. K. H., and Li, P. R.: A study on  
717 the aerosol extinction-to-backscatter ratio with combination of  
718 micro-pulse LIDAR and MODIS over Hong Kong, *Atmos. Chem. Phys.*,  
719 6, 3243-3256, 2006.

720 Henning, S., Wex, H., Hennig, T., Kiselev, A., Snider, J. R., Rose, D., et  
721 al.: Soluble mass, hygroscopic growth, and droplet activation of coated  
722 soot particles during LACIS Experiment in November (LExNo), *J.*  
723 *Geophys. Res.*, 115, D11206, doi: 10.1029/2009JD012626, 2010.

724 Herckes, P., Chang, H., Lee, T., and Collett Jr., J. L.: Air pollution  
725 processing by radiation fogs, *Water, Air, & Soil Pollution* 181 (1), 65-75,  
726 2007.

727 Hings, S. S., Wrobel, W. C., Cross, E. S., Worsnop, D. R., Davidovits, P.  
728 and Onasch, T. B.: CCN activation experiments with adipic acid: effect  
729 of particle phase and adipic acid coatings on soluble and insoluble  
730 particles, *Atmos. Chem. Phys.*, 8, 3735-3748, 2008.

731 Hitzenberger, R., Giebl, H., Petzold, A., Gysel, M., Nyeki, S.,  
732 Weingartner, E., Baltensperger, U., and Wilson, W. C.: Properties of jet  
733 engine combustor particles during the PartEmis experiment.  
734 Hygroscopic properties at supersaturated conditions, *Geophys. Res.  
735 Lett.*,30 (14), 1779, doi: 10.1029/2003GL017294, 2003.

736 Hudson, J.: Variability of the relationship between particle size and  
737 cloud-nucleating ability, *Geophys. Res. Lett.*, 34, L08801, doi:  
738 10.1029/2006GL028850, 2007.

739 Hudson, J. G. and Noble, S.: CCN and vertical velocity influence on  
740 droplet concentration and supersaturations in clean and polluted stratus  
741 clouds, *J. Atmos. Sci.*, 106, 24119-24126, 2014.

742 IPCC.: Climate Change 2007: The Physical Science Basis. In: Solomon,  
743 S., et al., (Eds.). Contribution of Working Group I to the Fourth  
744 Assessment Report of the Intergovernmental Panel on Climate Change,  
745 Cambridge Univ. Press, Cambridge and New York, 2007.

746 Jimenez, J. L. et al.: Evolution of organic aerosols in the atmosphere,  
747 *Science*, 326, 1525-1529, 2009.

748 Juranyi, Z., Gysel, M., Weingartner, E., DeCarlo, P. F., Kammermann, L.,

749 and Balternsperger, U.: Measurement and modeled cloud condensation  
750 nuclei concentration at the high alpine site Jungfraujoch, *Atmos. Chem.*  
751 *Phys. Discussions.*, 10, 8859-8897, 2010.

752 Köhler, H.: The nucleus in and the the growth of hygroscopic droplets, *T.*  
753 *Faraday Soc.*, 32, 1152-1161, 1936.

754 Kuang, C., McMurry, P. H., and McCormick, A.V.: Determination of  
755 cloud condensation nuclei production from measured new particle  
756 formation events, *Geophys. Res. Lett.*, 36, L09822, doi: 10.  
757 1029/2009GL037584, 2009.

758 Kuwata, M. and Kondo, Y.: Dependence of size-resolved CCN spectra on  
759 the mixing state of nonvolatile cores observed in Tokyo. *J. Geophys.*  
760 *Res.*, 113, D19202, doi; 10.1029/2007JD009761, 2008.

761 Kuwata, M., Kondo, Y., Mochida, M., Takegawa, N. and Kawamura, K.:  
762 Dependence of CCN activity of less volatile particles on the amount of  
763 coating observed in Tokyo, *J. Geophys. Res.*, 112, D11207, doi:  
764 10.1029/2006JD007758, 2007.

765 Lance, S., Medina, J., Smith, J. N., and Nenes, A.: Mapping the operation  
766 of the DMT Continuous Flow CCN counter, *Aerosol Sci. Tech.*, 40,  
767 242-254, 2006.

768 Lathem, T. L., and Nenes A.: Water vapor depletion in the DMT  
769 Continuous Flow CCN Chamber: Effects on supersaturation and droplet  
770 growth, *Aerosol Sci. Tech.*, 45(5), 604-615, 2011.

771 Leng, C. P., Cheng, T. T., Chen, J. M., et al.: Measurements of surface  
772 cloud condensation nuclei and aerosol activity in downtown Shanghai,  
773 *Atmos. Environ.*, 69, 354-361, 2013.

774 Liu, J. J., Zheng, Y. F., Li, Z. Q., and Cribb, M.: Analysis of cloud  
775 condensation nuclei properties at a polluted site in southeastern China  
776 during the AMF-China Campaign, *J. Geophys. Res.*, 116, D00K35, doi:  
777 10.1029/2011JD016395, 2011.

778 Lohmann, U. and Feichter, J.: Global indirect aerosol effect; a review,  
779 *Atmos. Chem. Phys.*, 5, 715-737, 2005.

780 Matsui, H., Koike, M., Kondo, Y., Takegawa, N., Fast, J. D., Pöschl, U.,  
781 Garland, R. M., Andreae, M. O., Wiedensohler, A., Sugimoto, N., and  
782 Zhu, T.: Spatial and temporal variations of aerosols around Beijing in  
783 summer 2006: 2. Local and column aerosol optical properties, *J.*  
784 *Geophys. Res.*, 115, D22207, doi: 10.1029/2010JD013895, 2010.

785 Menut, L., Flamant, C., Pelon, J., Flamant, P. H.: Urban boundary-layer  
786 height determination from lidar measurements over the Paris area. *Appl.*  
787 *Optics.* 38, 945-954, 1999.

788 Merikanto, J., Sprackken, D. V., Mann, G. W., Pickering, S. J and Carslaw,  
789 K. S.: Impact of nucleation on global CCN, *Atmos. Chem. Phys.*, 9(21),  
790 8601-8616, 2009.

791 Moffet, R. C., de Foy, B., Molina, L. T., Molina, M. J. and Prather, A.:  
792 Measurements of ambient aerosols in northern Mexico City by single

793 particle mass spectrometry, *Atmos. Chem. Phys.*, 8, 4499-4516, 2008.

794 Petters, M. D., and S. M. Kreidenweis.: A single parameter representation  
795 of hygroscopic growth and cloud condensation nucleus activity, *Atmos.*  
796 *Chem. Phys.*, 7, 1961-1971, 2007.

797 Petzold, A., Kopp, C. and Niessner R.: The dependence of the specific  
798 attenuation cross-section on black carbon mass fraction and particle  
799 size, *Atmos. Environ.*, 31(5), 661-672, 1997.

800 Pierce, J. R., et al.: Contribution of primary carbonaceous aerosol to  
801 cloud condensation nuclei: Processes and uncertainties evaluated with  
802 a global aerosol microphysics model, *Atmos.Chem. Phys.*, 7,  
803 5447-5466, doi: 10.5194/acp-7-5447-2007, 2007.

804 Qian, Y., Kaiser, D. P., Leung, L. R., and Xu, M.: More frequent  
805 cloud-free sky and less surface solar radiation in China from 1955-2000,  
806 *Geophys. Res. Lett.*, 33, L01812, doi:10.1029/2005GL024586, 2006.

807 Quinn, P. K., Bates, T. S., Coffman, D. J. and Covert, D. S.: Influence of  
808 particle size and chemistry on the cloud nucleating properties of aerosols,  
809 *Atmos. Chem. Phys.*, 8, 1029-1042, 2008.

810 Reade, L., Jennings, S. G., and Gobnait, M.: Cloud condensation nuclei  
811 measurements at Mace Head, Ireland, over the period 1994-2002, *Atmos.*  
812 *Res.*, 82, 610-621, 2006.

813 Ritesh, G., Christina, H., Menas. Kafatos., Si-Chee. T.: Influences of  
814 winter haze on fog/low cloud over the Indo-Gangetic plains. *J. Geophys.*

815 Res., 112, D05207, doi: 10. 1029/2005JD007036, 2007.

816 Roberts, G. C. and Nenes, A.: A continuous-flow streamwise  
817 thermal-gradient CCN chamber for atmospheric measurements, *Aerosol*  
818 *Sci. Tech.*, 39, 206-221, 2005.

819 Rose, D., Gunthe, S. S., Su. H., Carland. R. M., Yang. H., et al.: Cloud  
820 condensation nuclei in polluted air and biomass burning smoke near the  
821 mega-city Guangzhou, China- Part 2: Size-resolved aerosol chemical  
822 composition, diurnal cycles, and externally mixed weakly CCN-active  
823 soot particles, *Atmos. Chem. Phys.*, 11, 2817-2836, 2011.

824 Rose, D., Nowak, A., Achtert. P., Wiedensohler. A., Hu. M., et al.: Cloud  
825 condensation nuclei in polluted air and biomass burning smoke near the  
826 mega-city Guangzhou, China- Part 1: Size-resolved measurements and  
827 implications for the modeling of aerosol particle hygroscopicity and  
828 CCN activity, *Atmos. Chem. Phys.*, 10, 3365-3383, 2010.

829 Rosenfeld, D., Dai, J., Yu, X., Yao, Z., Xu, X., Wang, X., and Du, C.:  
830 Inverse relations between amounts of air pollution and orographic  
831 precipitation, *Science*, 315, 1396-1398, 2007.

832 Rosenfeld, D., Lohmann, U., Raga, G. B., O'Dowd, C. D., Kulmala, M.,  
833 Fuzzi, S., Reissell, A., and Andreae, M. O.: Flood or Drought: How Do  
834 Aerosol Affects Precipitation?, *Science*, 321, 5894, 2008.

835 Shao, M., Tang, X., Zhang, Y., and Li, W.: City clusters in China: air and  
836 surface water pollution, *Front. Ecol. Environ*, 4, 353-361, 2006.

837 Sihto, S. L., Mikkilä, J., Vanhanen, J., et al.: Seasonal variation of CCN  
838 concentrations and aerosols activation properties in boreal forest, *Atmos.*  
839 *Chem. Phys.*, 11, 13269-13285, 2011.

840 Stone, E. A., Snyder, D. C., Sheesley, R. J., Sullivan, A. P., Weber, R. J.  
841 and Schauer, J. J.: Source apportionment of fine organic aerosol in  
842 Mexico City during the MILAGRO experiment 2006, *Atmos. Chem.*  
843 *Phys.*, 8, 1249-1259, 2008.

844 Streets, D. G., Tsia, N. Y., Akimoto, H., and Oka, K.: Sulfur dioxide  
845 emissions in Asia in the period 1985-1997, *Atmos. Environ.*, 34,  
846 4413-4424, 2000.

847 Streets, D. G., Yu, C., Wu, Y., Chin, M., Zhao, Z., Hayasaka, T., and Shi,  
848 G.: Aerosol trends over China, 1980-2000, *Atmos. Res.*, 88, 174-182,  
849 2008.

850 Sun, Y. L., Zhuang, G. S., Tang, A. H., Wang, Y., and An, Z. S.: Chemical  
851 characteristics of PM<sub>2.5</sub> in haze-fog episodes in Beijing, *Environ. Sci.*  
852 *Tech.*, 40, 3148-3155, 2006.

853 Svenningsson, B., Rissler, J., Swietlicki, E., Mircea, M., Bilde, M., et al.:  
854 Hygroscopic growth and critical supersaturations for mixed aerosol  
855 particles of inorganic and organic compounds of atmospheric relevance,  
856 *Atmos. Chem. Phys.*, 6, 1937-1952, 2006.

857 Tie, X. and Cao, J.: Aerosol pollution in China: present and future impact  
858 on environment, *Particuology.*, 7, 426-43, 2009.

859 Urone, P., Lutsep, Helmut., Noyes. C. M., and Parcher, J. F.: Static  
860 studies of sulfur dioxide reactions in air, *Environ. Sci. Tech*, 2(8),  
861 611-618, 1968.

862 Wang, Y., Zhuang, G. S., Zhang, X. Y., Huang, K., Xu, C., Tang, A. H.,  
863 Chen, J. M., and An, Z. S.: The ion chemistry, seasonal cycle, and  
864 sources of PM<sub>2.5</sub> TSP aerosol in Shanghai, *Atmos. Environ.*,40,  
865 2935-2952, 2006.

866 Weingartner, E., Saathoff, H., Schnaiter, M., Streit, N., Bitnar, B., and  
867 Baltensperger U.: Absorption of light by soot particles: determination of  
868 the absorption coefficient by means of aethalometers, *J. Aerosol Sci.*, 34,  
869 1445-1463, 2003.

870 Wiedensohler, A., Cheng, Y. F., Nowak, A., Wehner. B., Achtert, P.,  
871 Berghof, M., Birmili, W., Wu, Z. J., et al.: Rapid aerosol growth and  
872 increase of cloud condensation nucleus activity by secondary aerosol  
873 formation and condensation: A case study for regional air pollution in  
874 northeastern China, *Geophys. Res. Lett.*,114, D00G08, doi:  
875 10.1029/2008JD010884, 2009.

876 Ye, X. N., Ma, Z., Zhang, J. C., Du, H. H., Chen, J. M., Chen, H., Yang,  
877 X., Gao, W., and Geng, F. H.: Important role of ammonia on haze  
878 formation in Shanghai, *Environ. Lett.*, 6, 024019, 2011.

879 Yu, F. Q., Wang, Z., Luo, G., and Turco, R.: Ion-mediated nucleation as  
880 an important global source of tropospheric aerosols, *Atmos. Chem.*



881 Phys., 8, 2537-2554, 2008.

882 Yue. D. L., Hu. M., Zhang. R. J., Wu. Z. J., Su. H., et al.: Potential  
883 contribution of new particle formation to cloud condensation nuclei in  
884 Beijing, Atmos. Environ., 45, 6070-6077, 2011.

885 Yum. S. S., James, G. H., Keun, Y. S., and Byoung-Cheol, C.:  
886 Springtime cloud condensation nuclei concentrations on the west coast  
887 of Korea, Geophys. Res. Lett., 32, L09814, doi: 10.  
888 1029/2005GL022641, 2005.

889 Yum. S. S., and James, G. H.: Wintertime/summertime contrasts of cloud  
890 condensation nuclei and cloud microphysics over the South Ocean, J.  
891 Geophys. Res., 109, D06204, doi: 10.1029/2003JD003864, 2004.

892 Zhang, M., Wang, X., Chen, J., Cheng, T., Wang, T. et al.: Physical  
893 characterization of aerosol particles during the Chinese New Year's  
894 firework events, Atmos. Environ., 44, 5191-5198, 2010a.

895 Zhang, Q., Tie, X. X., Lin, W. L., Cao, J. J., Quan, J. N., Ran, L., and Xu,  
896 W. Y.: Variability of SO<sub>2</sub> in an intensive fog in North China Plain:  
897 Evidence of high solubility of SO<sub>2</sub>, Particuology, 11, 41-47, 2013.

898 Zhang, R. J., Jing, J. S., Tao, J., Hsu, S.-C., Wang, G., Cao, J. J., Lee, C. S.  
899 L., et al.: Chemical characterization and source apportionment of PM<sub>2.5</sub>  
900 in Beijing: seasonal perspective, Atmos. Chem. Phys., 13, 7053-7074,  
901 2013.

902 Zhang, X. Y., Zhuang G. S., Chen, J. M., Wang, Y. X., An, Z. S., Zhang, P.:

903 Heterogeneous reactions of sulfur dioxide on typical mineral particles, J.

904 Phys. Chem., B, 110, 12588-12596, 2006b.

905

906

907

908

909

910

911

912

913

914

915

916

917

918

919

920

921

922

923

924

925 **Table 1** Statistics of meteorological parameters in different weather  
 926 conditions.

	Clear day	Foggy-hazy day	Hazy day	All
Temperature ( °C)	14.39	14.59	16.53	15.02
Wind direction (deg)	157.22	191.36	260.59	191.27
Wind speed (m/s)	1.95	1.28	2.27	1.94
Pressure (hPa)	1021.92	1019.19	1019.45	1020.83
RH (%)	58.13	84.93	58.33	61.95
Visibility (km)	15.41	2.33	4.44	10.42
PBL (km)	1.2	0.58	0.62	0.93
Extinction coefficient	0.32	0.27	0.76	0.62

927  
 928 **Table 2** Statistics of CCN, CN, CCN/CN and BC in different weather  
 929 conditions.

	Clear day	Foggy-hazy day	Hazy day	All
CCN range (cm <sup>-3</sup> )	994-5096	1677-2947	2088-6268	994-6268
CCN average (cm <sup>-3</sup> )	2432	2377	4362	2929
CN range (cm <sup>-3</sup> )	4270-15,168	4815-13,922	6033-15,771	4270-15,771
CN average (cm <sup>-3</sup> )	8956	8367	10500	9344
CCN/CN range	0.09-0.48	0.18-0.40	0.25-0.57	0.09-0.57
CCN/CN average	0.28	0.29	0.41	0.32
BC range (µg/m <sup>-3</sup> )	4.51-20.40	6.7-14.7	8.3-35.2	4.51-35.20
BC average (µg/m <sup>-3</sup> )	8.57	9.58	21.26	12.24

930  
 931  
 932 **Table 3** Effective hygroscopicity parameters ( $\kappa_i$ ), and densities of the  
 933 three category compositions in fine particles (Yue et al., 2011)

Species	Data source	$\kappa_i$	Density (g cm <sup>-3</sup> )
Sulfate & Nitrate	SO <sub>4</sub> <sup>2-</sup> +NO <sub>3</sub> <sup>-</sup> +NH <sub>4</sub> <sup>+</sup>	0.6	1.7
Sodium chloride and marine aerosols	Na <sup>+</sup> +Cl <sup>-</sup>	1.0	2.2
Insoluble compounds	BC	0	1.0
	others	0	2.0

934

935 **Figure captions**

936

937 **Figure 1** Agricultural fire scattering areas and air mass transport  
938 pathways across these regions. All red spots represent biomass burning  
939 sites on 7 November measured from MODIS satellite. Starting time (LT)  
940 is labeled in the figure.

941 **Figure 2** Temporal variations of temperature, wind speed and direction,  
942 RH, pressure and atmospheric visibility.

943 **Figure 3** Temporal variations of PBL and vertical extinction coefficient  
944 measured by MPL lidar.

945 **Figure 4** Hourly mean particle number concentrations of different  
946 sub-size bins.

947 **Figure 5** Average size distributions for all the hazy, foggy-hazy, and clear  
948 cases.

949 **Figure 6** Temporal variations of particle water soluble ion composition  
950 and trace gases.

951 **Figure 7** Temporal variations of  $N_{CN}$ ,  $N_{CCN}$  at 0.2% SS, BC,  $PM_{2.5}$  and  
952  $N_{CCN}/N_{CN}$ .

953 **Figure 8** Temporal variations of  $CN_{100nm-10\mu m}$ ,  $CN_{80nm-10\mu m}$ ,  $CCN/$   
954  $CN_{100nm-10\mu m}$  at 0.2% SS and  $CCN/ CN_{80nm-10\mu m}$  at 0.2% SS.

955 **Figure 9** Correlations of BC mass concentration ( $M_{BC}$ ) to  $N_{CCN}$  and  
956  $N_{CCN}/N_{CN}$  (0.2% SS).

957 **Figure 10** Scatterplot of the simplified closure analysis at SS 0.2%.

958 **Figure 11** Correlations of observed and predicted  $N_{CCN}$  (0.2% SS) in the  
959 clear (a) and foggy-hazy/hazy (b) cases.

960

961

962

963

964

965

966

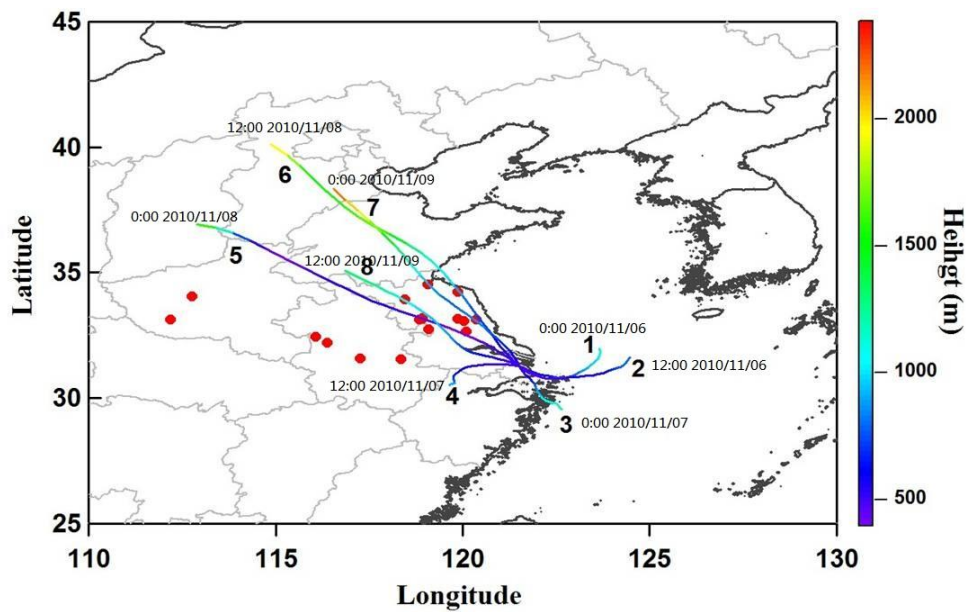
967

968

969

970

971



972

973 **Figure 1** Agricultural fire scattering areas and air mass transport  
 974 pathways across these regions. All red spots represent biomass burning  
 975 sites on 7 November measured from MODIS satellite. Starting time (LT)  
 976 is labeled in the figure.

977

978

979

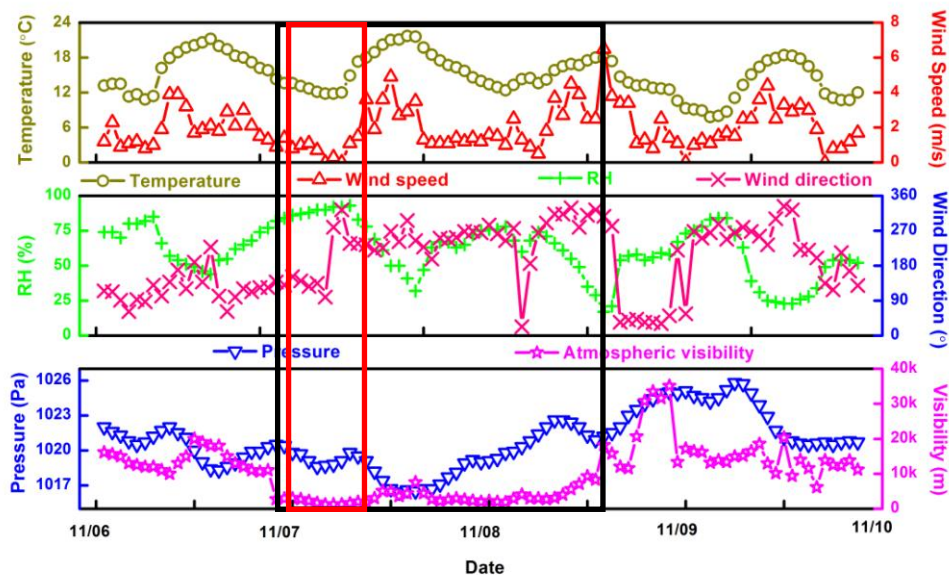
980

981

982

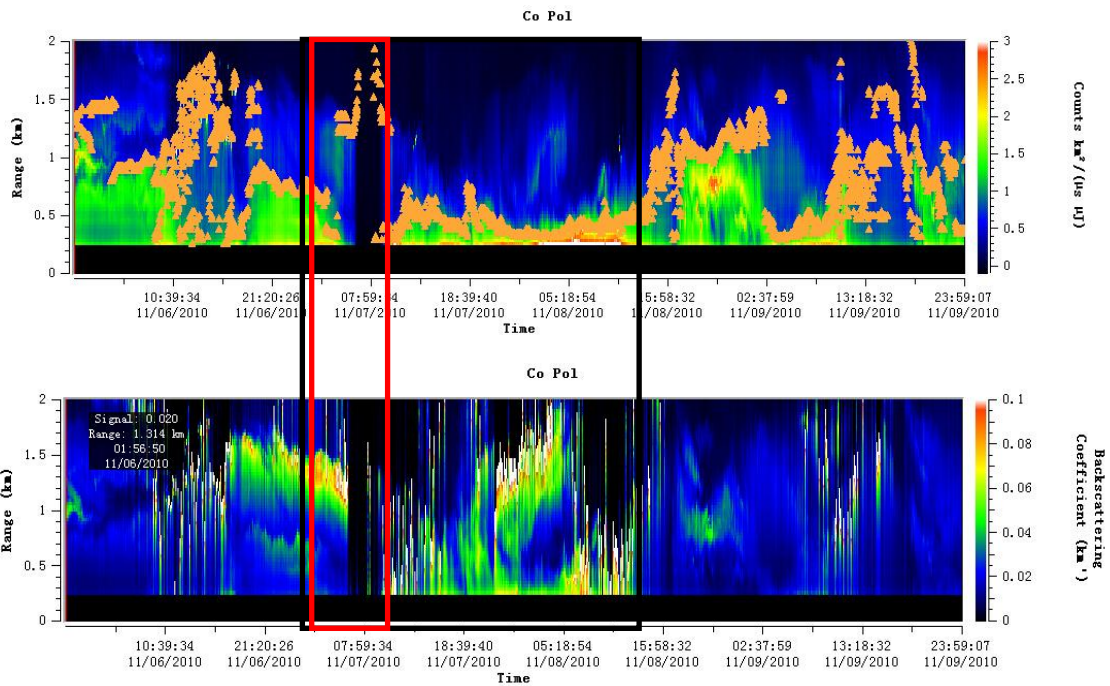
983

984



985 **Figure 2** Temporal variations of temperature, wind speed and direction,  
 986 RH, pressure and atmospheric visibility.

987



988

989

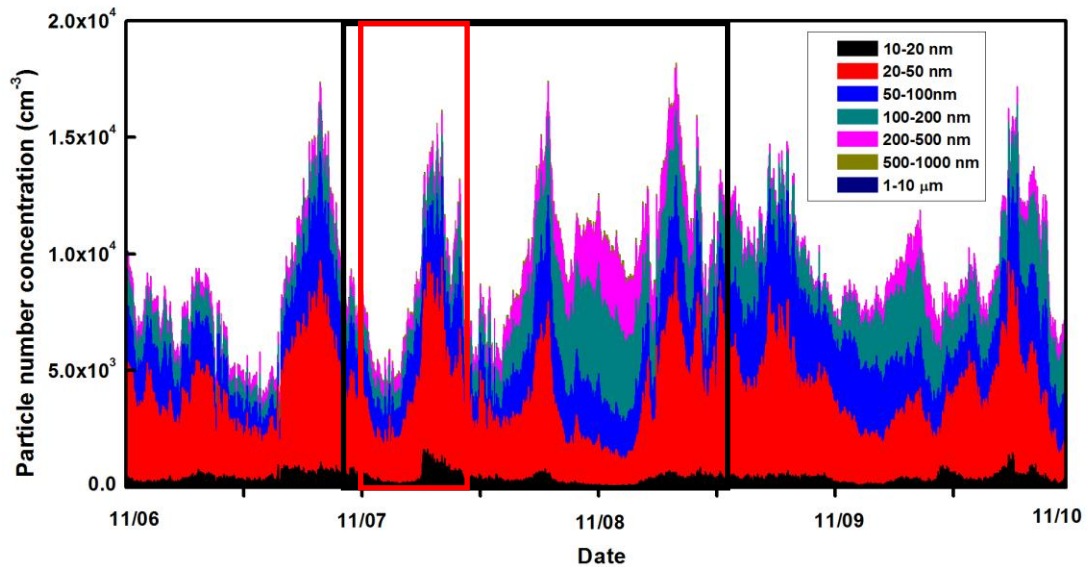
990

991 **Figure 3** Temporal variations of PBL and vertical extinction coefficient

992 measured by MPL lidar.

993

994



995

996

997

998

999

1000

1001

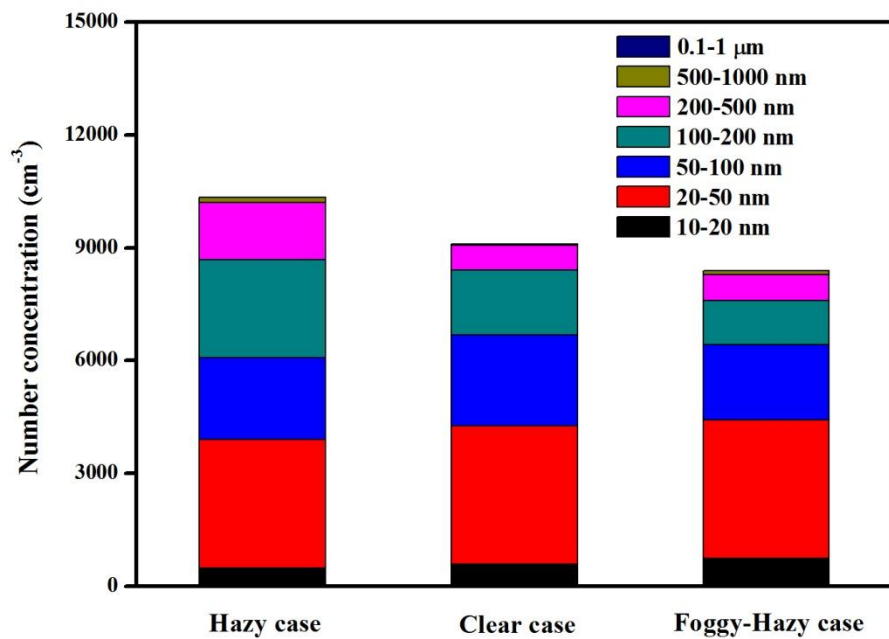
1002

1003

1004

**Figure 4** Hourly mean particle number concentrations of different

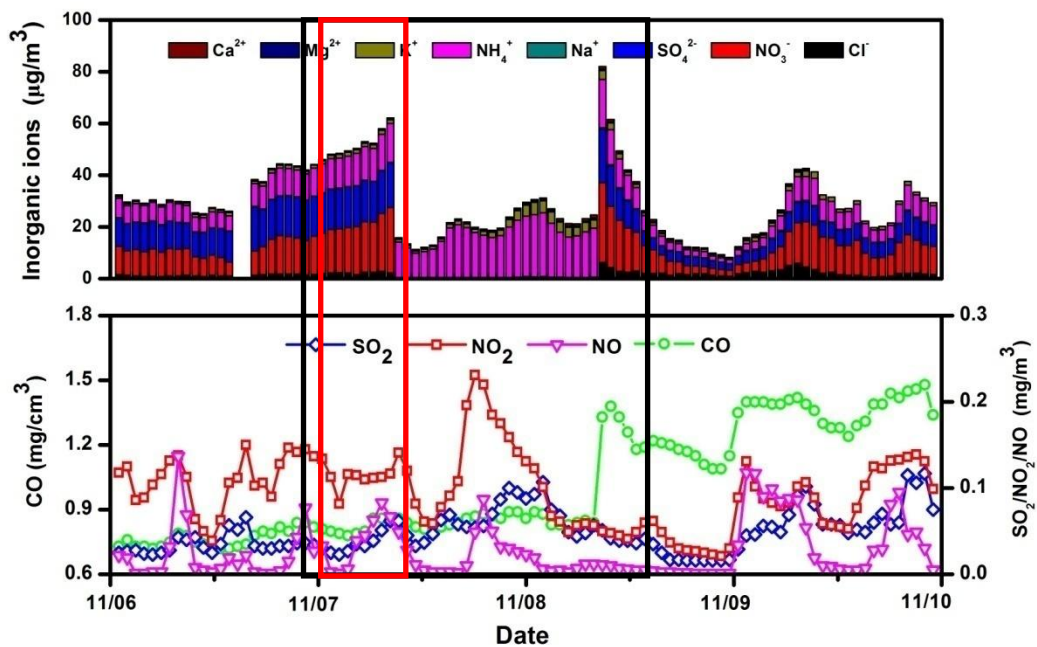
sub-size bins.



1005

1006 **Figure 5** Average size distributions for all the hazy, foggy-hazy, and clear

1007 cases.



1008

1009 **Figure 6** Temporal variations of particle water soluble ion composition

1010 and trace gases.



1011

1012

1013

1014

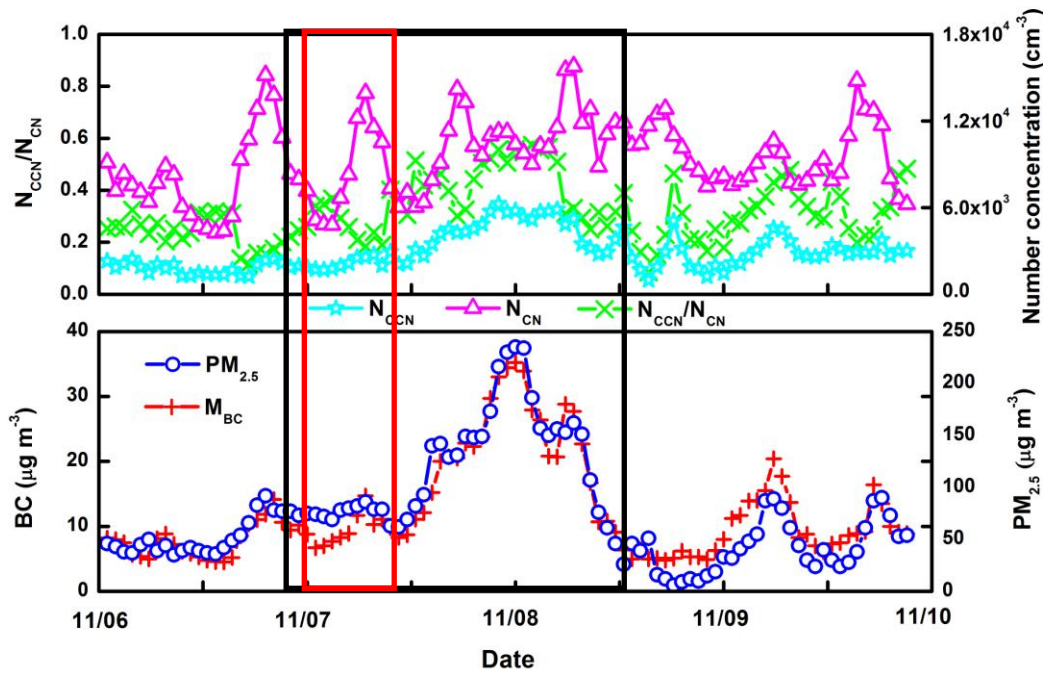
1015

1016

1017

1018

1019



1020 **Figure 7** Temporal variations of  $N_{CN}$ ,  $N_{CCN}$  at 0.2% SS, BC,  $PM_{2.5}$  and

1021  $N_{CCN}/N_{CN}$ .

1022

1023

1024

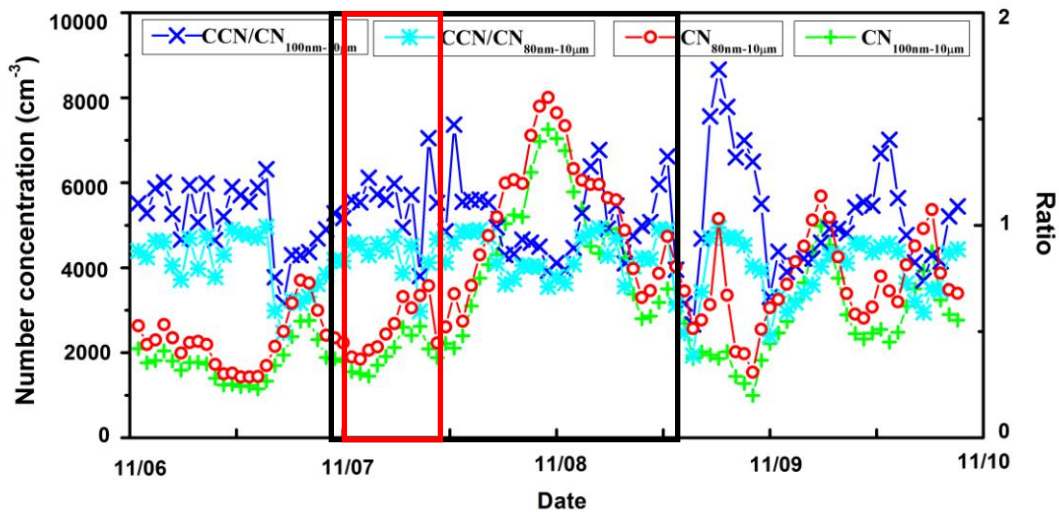
1025

1026

1027

1028

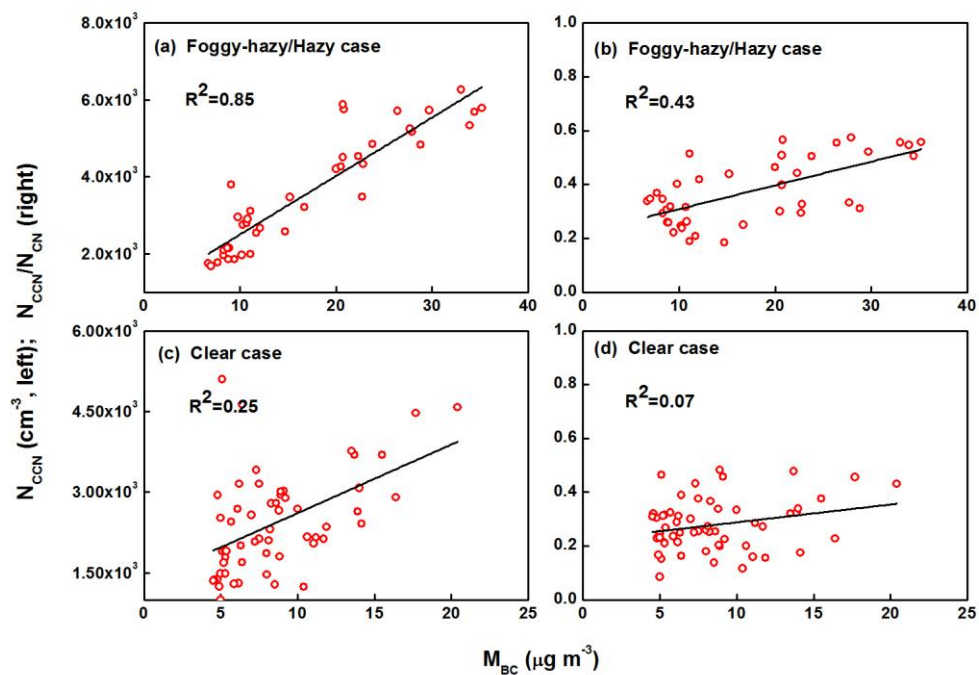
1029



1030 **Figure 8** Temporal variations of  $CN_{100nm-10\mu m}$ ,  $CN_{80nm-10\mu m}$ ,  $CCN/$

1031  $CN_{100nm-10\mu m}$  at 0.2% SS and  $CCN/ CN_{80nm-10\mu m}$  at 0.2% SS.

1032

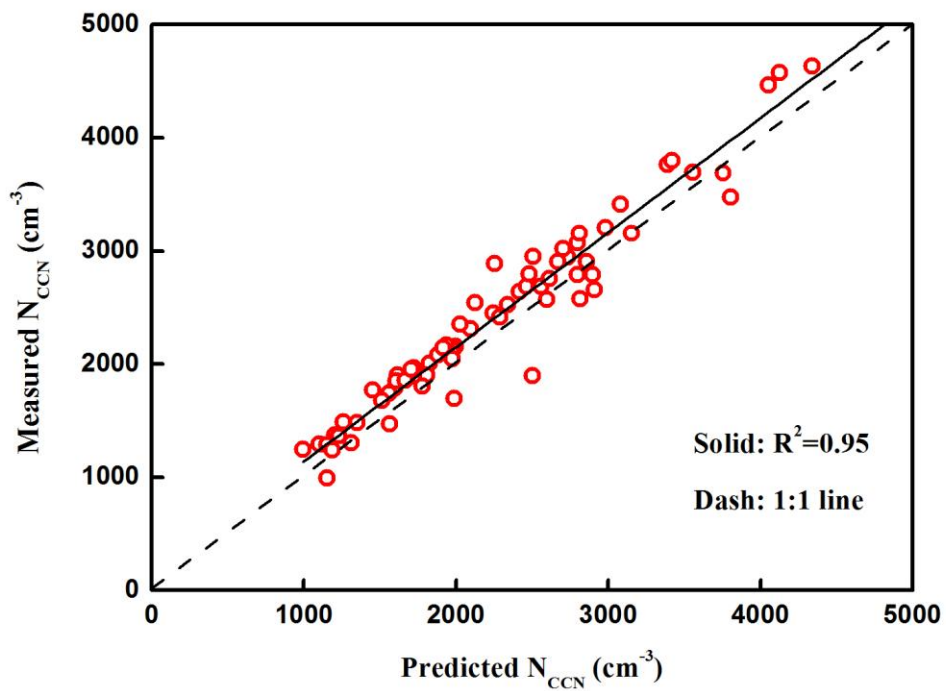


1033

1034 **Figure 9** Correlations of BC mass concentration ( $M_{BC}$ ) to  $N_{CCN}$  and

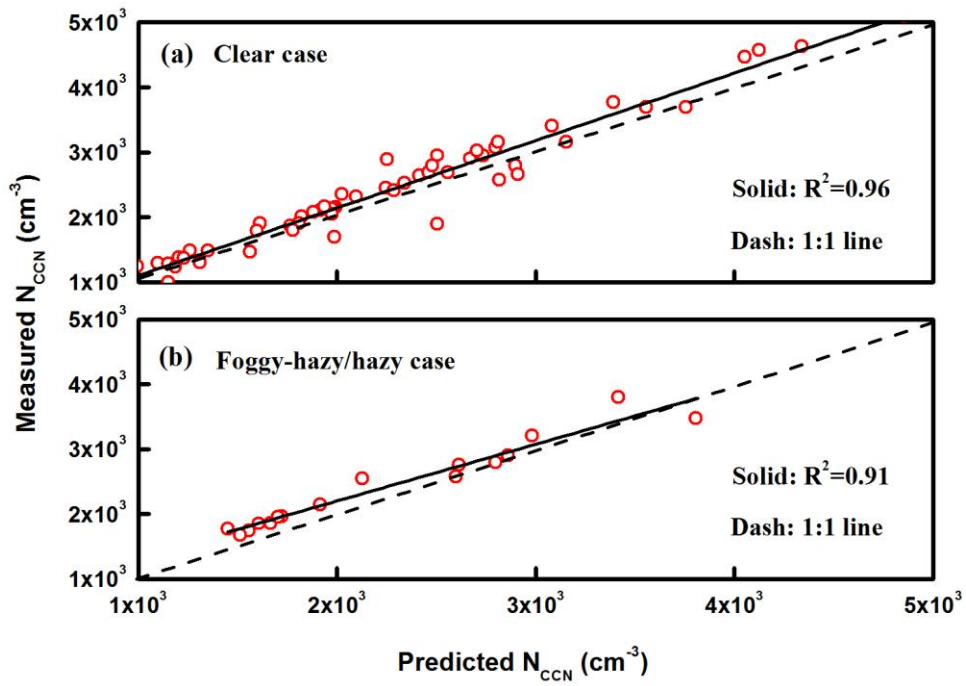
1035  $N_{CCN}/N_{CN}$  (0.2% SS).

1036



1037

1038 **Figure 10** Scatterplot of the simplified closure analysis at SS 0.2%.



1039

1040 **Figure 11** Correlations of observed and predicted  $N_{CCN}$  (0.2% SS) in the  
 1041 clear (a) and foggy-hazy/hazy (b) cases.

1042

1043